I.P.N. BP n°1 – 91406 ORSAY

institut de physique nucléaire CNRS - IN2P3 - UNIVERSITÉ PARIS - SUD

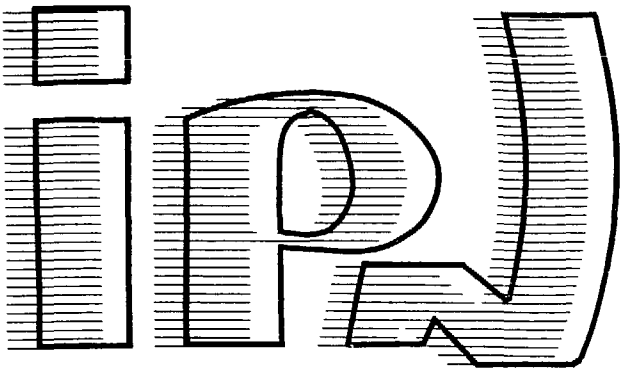

IPNO DRE 89-46

Deep inelastic transfers : a way to dissipate energy and angular momentum for reactions in the Fermi energy domain.

L. Tassan-Got and C. Stéphan

Institut de Physique Nucléaire 91406 Orsay France

1|2

Deep inelastic transfers : a way to dissipate energy and angular momentum for reactions in the Fermi energy domain

L. Tassan-Got and C. Stéphan

Institut de Physique Nucléaire 91406 ORSAY Cedex, France

Short title : Dissipative transfers in the Fermi energy domain

Résumé

Un modèle de transferts stochastiques de nucléons, utilisant une méthode Monte Carlo et prenant en compte la désexcitation séquentielle des fragments, a été élaboré et appliqué à des réactions pour des énergies voisines de l'énergie de Fermi : entre 27 et 44 MeV-A. Ses résultats ont été comparés à un large ensemble de données expérimentales : spectres en énergie, corrélations entre quasi-projectile et quasi-cible, distributions isotopiques, multiplicités de neutrons. Le modèle reproduit correctement de nombreux aspects de ces réactions. Au-delà de cet accord général, il est nécessaire de modifier la description des transferts en incluant la possibilité d'une émission de prééquilibre.

Abstract

A model of stochastic transfers, using a Monte Carlo method and accounting for sequential evaporation, has been elaborated and applied to reactions in the Fermi energy range : between 27 and 44 MeV-A. Its results have been compared to a large set of experimental data : energy spectra, correlations between projectile-like and target-like products, isotopic distributions, neutron multiplicities. Major features of these reactions are reproduced. Beyond this agreement, a modification of the transfer mechanism is needed to incorporate preequilibrium emission.

1. Introduction

For several years, heavy ion reactions at bombarding energy in the vicinity of the Fermi energy (typically from 15 to 40 MeV-A), have been analysed in the framework of fragmentation process or participant-spectator model [1–3]. Three main arguments lead to this kind of interpretation :

i) velocity spectra of projectile-like fragments detected below or at the grazing angle are peaked at velocities close to the projectile one. This observation has been taken as an evidence for the low excitation energy stored in the fragments,

ii) the yield of fragments heavier than projectile is suppressed and this has been considered as a signature of the disappearence of transfer mechanisms,

iii) isotopic distributions for ^{40}Ar projectiles were found similar to those obtained at higher bombarding energies, almost independent of the target.

We state that the experimental findings, listed above, are not strong indications for the onset of fragmentation and the fading of transfer mechanisms well known in deep inelastic reactions at lower bombarding energies.

Concerning argument *i)*, from velocity spectra, one can try to extract Q-values assuming two-body kinematics. For example, in the case of the ^{34}S nucleus produced in the reaction ^{40}Ar + ^{58}Ni at 26.5 MeV-A [4], one finds $Q = -125$ MeV for the so-called "fragmentation peak", which does not correspond to a really low excitation energy. The paradox originates from the fact that, at fixed dissipated energy, the higher the incident velocity, the lower the relative shift of the fragment velocity. Bearing in mind that the excitation energy may be high, statements *ii)* and *iii)* are easily understood, even in the pure transfer mechanism framework, as effects of particle emission through evaporative processes.

Indeed, later experiments [5] directly showed that nuclei produced in these reactions are highly heated. Other experiments with heavier projectiles [6] like ^{86}Kr confirmed, through the significant yield of Z's higher than the projectile one, the presence of a transfer mechanism. This was possible in this case because the heavy products mainly deexcite by neutron evaporation, keeping memory of proton transfers, unlike lighter projectiles.

It is widely admitted now that energy dissipation occurs in heavy ion reactions until at least 60 MeV-A incident energy, and that it is a common feature of these reactions. This lead to the elaboration of models including transfers to generate energy dissipation, and associating this mechanism to a fragmentation step[7].

In order to appreciate the necessity to call upon a fragmentation process, we addressed the following questions : are deep inelastic transfers able to explain the main results related to the reactions in the Fermi energy range ? What is the meaning of the discrepancies that will show up ? To answer these questions we attempted to compare a wide variety of experimental results to the predictions of a model describing the energy and angular momentum dissipation as generated by successive nucleon transfers. In its spirit, the model is similar to the one elaborated by *Samaddar et al.*[8]. The main differences are that, in our case, we take the angular momentum into account for the transfer probabilities and the friction force for the relative motion directly arises from the simulated transfers. The model gives good results for lower bombarding energies ($\geq$ 8 MeV-A) and is now applied without any modification to reactions in the Fermi energy domain. This model has already been described elsewhere[9] and we only recall here its main ingredients. This is the purpose of the next section. Section 3 is devoted to the comparison to experimental results and, finally, we draw some conclusions in Section 4.

2. Description of the model

We assume, as in *Randrup*'s theory[10], that dissipation mainly proceeds through stochastic transfers of nucleons. These transfers are decoupled in time and the involved nucleons are treated at the classical limit. Nuclei are supposed to move along classical trajectories. When they come close to each other, a window defined by potential barriers opens and stochastic transfers may occur. These transfers generate dissipation and fluctuations. In the model, this aspect is simulated by random drawing leading to a Monte Carlo method which allows to compute any observable on an event by event basis.

Playing the game of full energy conservation, one gets the following equation for the variations of different kinds of energy :

$$\Delta\delta_1 + \Delta\delta_2 + \Delta E_1^* + \Delta E_2^* + \Delta K + \Delta U = 0 \qquad (1)$$

The first two terms account for the variations of the mass excesses of the two nuclei in their ground states. They are deduced from mass tables. The two following ones are evaluated by :

$$\begin{aligned} \Delta E_1^* &= \epsilon_{F1} - \epsilon_1 \\ \Delta E_2^* &= \epsilon_2 - \epsilon_{F2'} \end{aligned} \tag{2}$$

where ϵ_1 and ϵ_2 are the energies of the transferred nucleon referred to nuclei 1 (donor) and 2 (acceptor); ϵ_{F1} and $\epsilon_{F2'}$ are the Fermi energy levels, the *prime* sign $'$ labelling the nucleus 2 *after* it received the transferred nucleon (figure 1). We shall also define ϵ_{1x} as the kinetic energy associated to the velocity component which is perpendicular to the separation window.

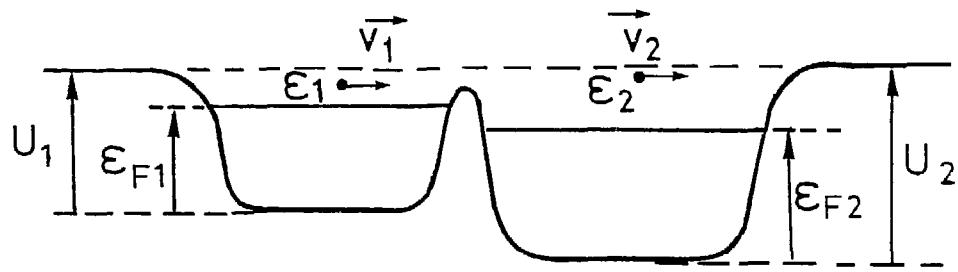

Figure 1

Definition of constants relative to each potential well. Energies of the transferred nucleon are kinetic energies referred to each potential well.

The last two terms of equation (1) are the variations of relative kinetic energy and potential of the composite system, this last quantity being sizeable only for proton transfers due to the long range coulomb interaction.

From (1) and (2) we derive :

$$\Delta K = -\Delta U - (\epsilon_2 - \epsilon_1) \tag{3}$$

If S_1 and S_2 are the spins of colliding nuclei and L the relative angular momentum, we get also :

$$\begin{aligned} \Delta S_1 &= -m_1 \\ \Delta S_2 &= m_2 \\ \Delta L &= -(m_2 - m_1) \end{aligned} \tag{4}$$

where m_1 and m_2 are the angular momenta of the transferred nucleon respectively to nuclei 1 and 2.

In order to couple ϵ_2 and m_2 to ϵ_1 and m_1 and then use equations (2)-(4), we adopted a velocity shift prescription :

$$\begin{aligned} \vec{v}_{02} &= \vec{v}_1 + \vec{V}_r \\ \epsilon_2 &= \frac{1}{2} m_0 v_{02}^2 - \Delta U \end{aligned} \tag{5}$$

where $\vec{V}_r$ is the relative velocity. This prescription slightly differs from *Randrup*'s one by the potential term which reflects that the velocity of the transferred nucleon is only affected by the potential variation associated to the transfer. This added term is necessary for detailed energy conservation in the case of proton transfer, due to the long range Coulomb force.

Then the transfer is described at the classical limit by 5 parameters :

$$\sigma \left| \begin{array}{l} \epsilon_1 \\ \lambda = \sqrt{\dfrac{\epsilon_{1x}}{\epsilon_1}} \\ \mu = \dfrac{m_1}{r_1 \sqrt{2 m_0 \epsilon_1}} \\ \rho \\ \theta \end{array} \right. \begin{array}{l} \\ \Big\} \text{ velocity components} \\ \\ \Big\} \text{ location on the window (figure 2)} \end{array}$$

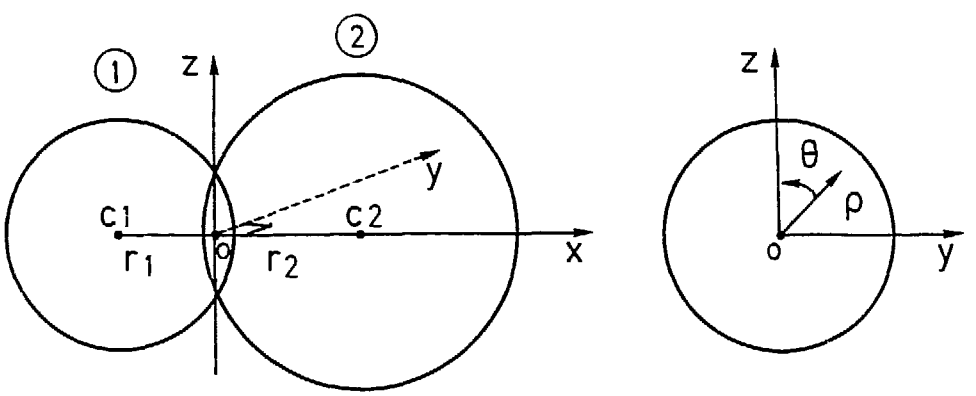

Figure 2

Geometric characterization of the system. The relative velocity $\vec{V}_r$ of nucleus 2 referred to 1 is in the (Ox,Oy) plane, with a positive Oy projection. ρ and θ are used to localize the transfer in the window.

All the relevant defined quantities can be expressed as functions of these parameters, at first ϵ_2, m_1, m_2, and then from equations (2)-(4) all the variations of angular momentum and energies.

To go further we need the computation of transfer probabilities. For this goal we use a phase space formula accounting for Pauli blocking comparable to the one used by *Samaddar et al.*[8] :

$$\mathrm{P} = \int d^5\sigma \; \Phi \; T \, n_1 \, (1 - n_2) \tag{6}$$

- Φ : is a one-way local flux (phase space flux) calculated in the classical limit approximation including energy and angular momentum. From the usual hitting rate per time and area units :

$$\frac{dn}{dS\,dt} = \frac{2}{h^3} v_z \, d^3\vec{p}$$

where the factor 2 is for the spin degeneracy, one derives :

$$\Phi \; d^5\sigma = c \, \frac{8 m_0 c^2}{(2\pi\hbar c)^3} \, \frac{\epsilon_1 \; \lambda \, d\lambda \, d\mu \, d\epsilon_1}{\sqrt{1 - \lambda^2 - \left(\mu + \lambda \frac{\rho}{r_1} \sin\theta\right)^2}} \, \rho \, d\rho \, d\theta$$

with $0 \leq \lambda \leq 1$,

- T : is a barrier penetrability depending on the particle potential at the window, calculated as the addition of Saxon-Woods nuclear potentials and eventually Coulomb interaction. For the computation of T we used *Hill-Wheeler* formula for parabolic barriers,
- n_i : are occupation probabilities for equilibrated systems including angular momentum distortion due to spins of nuclei :

$$n_i = \frac{1}{1 + \exp\left(\frac{\epsilon_i - \epsilon_{Fi} - S_i m_i / I_i}{T_i}\right)} \qquad I_i = \text{moment of inertia}$$

The relative motion is described by steps as a conservative motion (without friction). At each step the probability (6) is evaluated for the 4 possible transfers and a random number is drawn. If the transfer occurs, its characteristics are also decided by random drawing according to partial probability given by the integrand of equation (6). The constants of the system are then reajusted and the process is continued.

This procedure generates highly excited primary events. As an example for the reaction $^{40}\mathrm{Ar} + {}^{197}\mathrm{Au}$ at 27 MeV-A, each transferred nucleon carries, on average, 27 MeV. After ten transfers, which is a typical value, the excitation energy stored in the system exceeds 250 MeV. We applied an evaporation code taking only account of neutron, proton and alpha emission. At

this step too, a Monte Carlo method is used and we get secondary events which can be directly compared to experimental results.

Several hypotheses have been assumed although we know that they are not thoroughly fulfilled. As an example, statistical equilibrium of each partner is doubtful but we may hope this is not relevant for the computation of transition probabilities as the effect of the high relative velocity is much greater than detailed state of each nucleus. For the same reason the decoupling in time of the reaction step and the evaporative step should not affect the results. On the contrary the neglect of preequilibrium emission, other dissipative processes and of other decay modes, like composite fragment emission, are not justified and should have to be included. We consider that the model is only a first attempt to analyse experimental data in the framework of deep inelastic collisions.

We want to stress that two-body collisions are not explicitly treated, but they are implicitly assumed as they must be present to dispatch in the two nuclei the energy and angular momentum carried on by the transferred nucleons. Without two-body collisions most of the transferred nucleons would escape from the system giving rise to preequilibrium emission, due to the high relative velocity.

Finally we mention that a threshold has been set for the maximum overlap of the nuclear densities. When this overlap is greater than 3 fm, the event is rejected. This value is arbitrary but it only affects events associated with very high excitation energy leading to low masses after the evaporation step. In that sense the model is only suited for "peripheral" reactions.

3. Comparison to experimental results

3.1. Energy and momentum spectra

The Monte Carlo method allows to calculate not only mean values and widths but also the very spectra. It is interesting to look at velocity spectra, or equivalently energy spectra, as their characteristics were often retained as clues of the fragmentation process.

On figure 3 are displayed the calculated energy spectra (heavy dots) for ^{34}S and ^{25}Mg isotopes for the reaction $^{40}Ar + ^{58}Ni$ at 26.5 MeV-A. The experimental results are represented by the histogram [4]. It must be noticed that *no normalisation factor* is used, the differential cross section is given by the simulation.

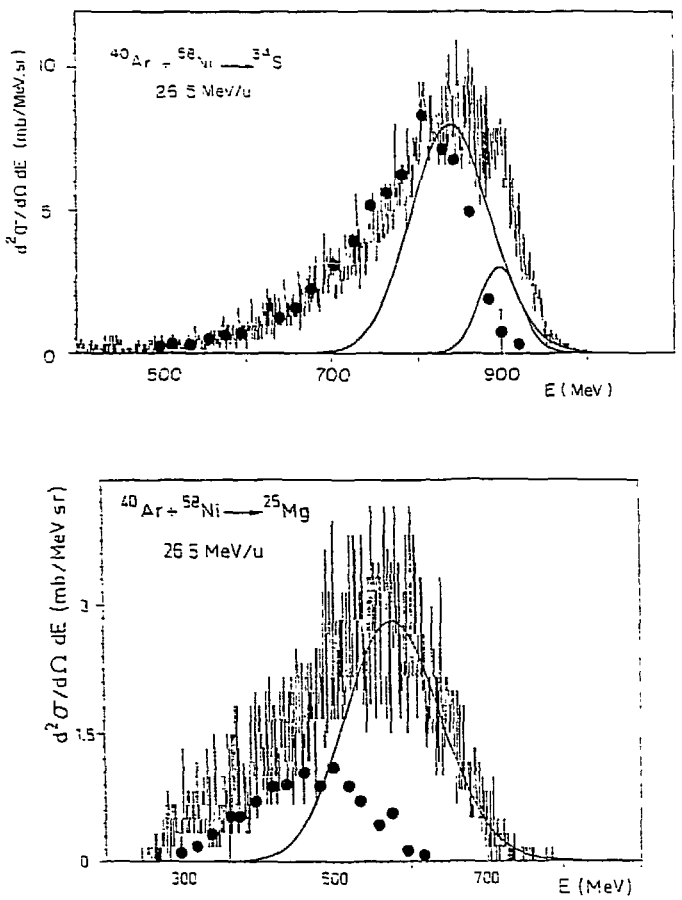

Figure 3

Energy spectra of ^{34}S and ^{25}Mg detected at 4° in the reaction $^{40}Ar + ^{58}Ni$ at 26.5 MeV-A. Histograms are experimental spectra[4]. The dots ● give the simulation results without any renormalization.

The first evidence is that the shape of these spectra is well reproduced, especially their skewness associated to the low energy tail. The absolute value is satisfactory when the detected fragments are not too far away from the projectile.

Secondly, high velocities are found for the projectile-like fragments, close to the projectile one. Although we applied a mechanism which is ordinarily suited for describing deep inelastic reactions, we get no cross section in the vicinity of the coulomb barrier which is located out of the frame (on the left side) in figure 3. This can be easily explained : due to the narrow mass distribution of primary events, selecting one detected fragment is equivalent to a selection in excitation energy through particle evaporation. By this way, the total kinetic energy loss has an upper bound reflected by the high velocities which result from the calculations.

The position of the maximum in the energy spectra is slightly shifted towards a lower energy, if compared to the experimental one. This energy shift becomes larger when the fragment charge is decreased. This systematic trend is shown in figure 4 where the position of this maximum is plotted as a function of the detected mass. Figure 5 displays the calculated mean values (stars) of the energy spectra for the $^{40}Ar + ^{27}Al$ system at 44 MeV-A [2]. In this latter case, the agreement is better if one notes that the energy scale is expanded. However the same general behaviour

as for the $^{40}Ar + ^{58}Ni$ system is still present. The full line is the prediction of the dissipative fragmentation model[7].

In order to explain the discrepancy, it is necessary to invoke less dissipative processes. One may think of fragmentation. Another way would be to take account of the possibility for transferred nucleons to escape from the acceptor nucleus after having deposited only a part of the kinetic energy they carry on. Such a process, which would lead to preequilibrium emission, is likely to occur as the transferred nucleon velocity is high in the acceptor nucleus. It would imply a decrease of the two partner masses without full momentum transfer by the involved nucleons.

The interpretation of reactions in the framework of fragmentation models often lead to the study of parallel ($\sigma_{\parallel}$) and perpendicular ($\sigma_{\perp}$) linear momentum widths. The comparison is usually done to *Goldhaber's* model[11] which relates the momentum widths to the Fermi momentum of nucleons and derives a parabolic dependence on the fragment mass. If the agree-

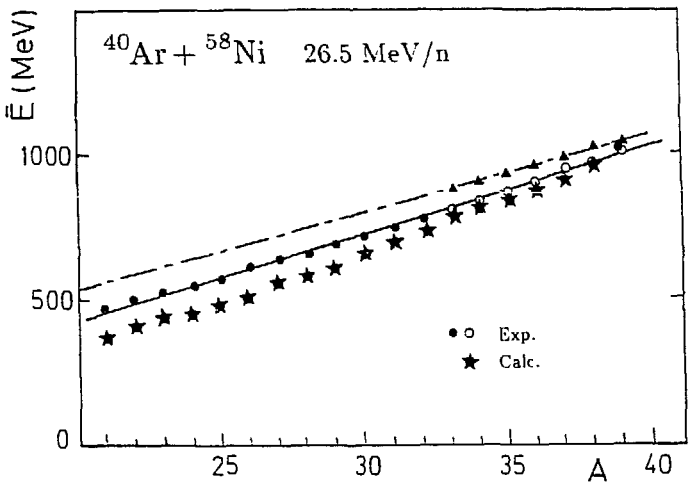

Figure 4

Most probable fragment energy $\bar{E}$ as a function of its mass A. Measurements were obtained at $\theta_{lab} = 4°$ for the $^{40}Ar + ^{58}Ni$ system at 26.5 MeV-A. Dots • and circles ○ are for experiment[4] and stars ★ for the simulation results.

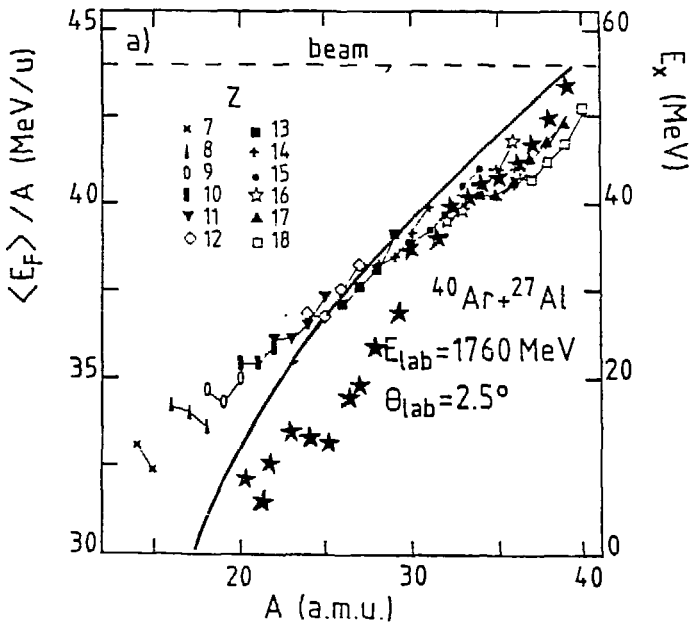

Figure 5

Mean fragment energy per nucleon $\langle E_F \rangle / A$ as a function of its mass A. Data are obtained at 2.5° for $^{40}Ar + ^{27}Al$ at 44 MeV-A[2]. Simulation is represented by stars ★, and the full line indicates Bonasera et al. calculation[7].

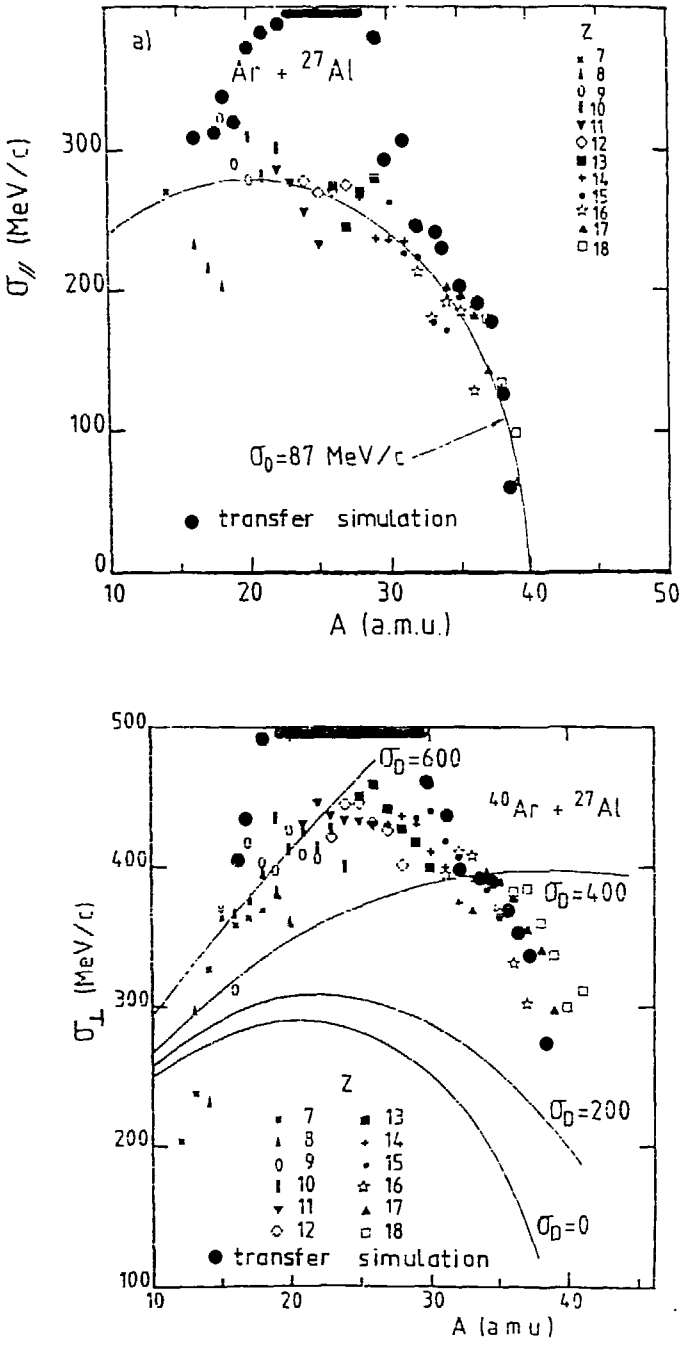

Figure 6

Widths of parallel (top) and perpendicular (bottom) linear momenta versus the detected fragment mass in the reaction $^{40}Ar + ^{27}Al$ at 44 MeV-A [2]. Dots ●, and thick full line when values were too high, are for results from simulation.

ment is generally good for parallel widths, it is not the case for perpendicular ones, experimental values being larger than theoretical ones. We tried to extract calculated momentum widths for the reaction $^{40}Ar + ^{27}Al$ at 44 MeV-A using the same prescriptions as for experimental widths[2]. The results for $\sigma_{\parallel}$ and $\sigma_{\perp}$ are displayed in figure 6 where heavy dots indicate the calculated values. The agreement is good for $30 \leq A \leq 40$ but for lower masses the model overestimates the experimental widths by a factor of 2 at maximum (the thick horizontal bars at the top of the figure indicate that the calculated points lie out of the frame). It is interesting to note that it is precisely for $A < 30$ that an energy dissipation excess is growing up. As dissipation and fluctuations are related, this excess is reflected in the larger widths coming out of the calculations. Nevertheless, for masses higher than 30, the model predictions are satisfactory and the differences between $\sigma_{\parallel}$ and $\sigma_{\perp}$ receive a natural interpretation.

3.2. Correlations between projectile-like target-like fragments

Several experiments aimed at measuring the correlation between projectile-like and target-like fragments. In this comparison we shall concentrate on the $^{40}Ar + ^{nat}Ag$ system which was studied at two close bombarding energies : 30 MeV-A[12] and 27 MeV-A[13] in slightly different conditions.

In order to compare the simulation with the experimental results, we applied the evaporation code to the target-like fragment coming out from the calculations. As for the projectile decay, kinematical effects of the evaporation (recoil momentum) are taken into account.

Figure 7 displays the comparison for the correlation between the two masses (A_P– $< A_T >$ correlation) at 30 MeV-A. Figure 8 shows a similar comparison, but with the projectile-like charge (Z_P– $<A_T>$ correlation) for the lower energy. In this case the projectile-like fragments were detected for three different

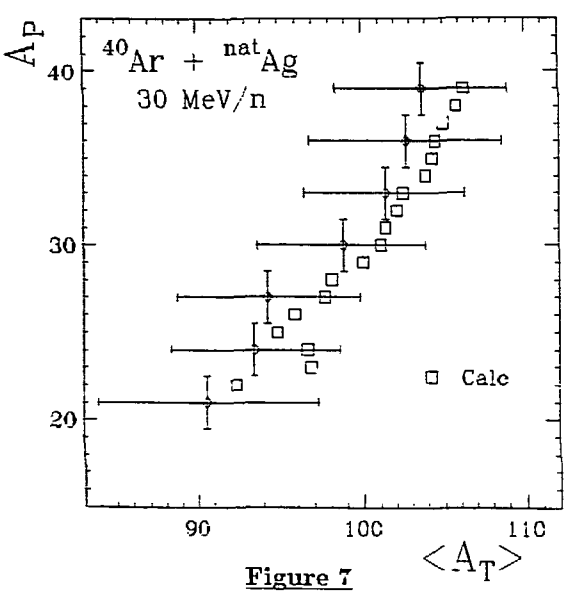

Figure 7

Correlation between projectile-like mass A_P and mean target-like mass $< A_T >$ for the reaction $^{40}Ar + ^{nat}Ag$ at 30 MeV-A. ◇ give experimental values[12]. The associated vertical bars show the selected bins while horizontal ones indicate the standard deviation of the corresponding target-like mass spectra. Squares □ are from simulation.

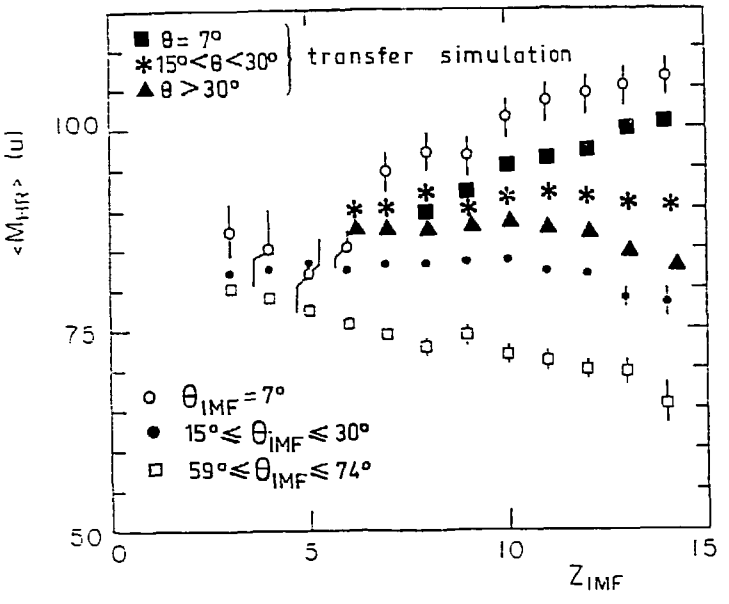

Figure 8

*Correlation between projectile-like atomic number Z_{IMF} and mean target-like mass $<M_{HR}>$ for the $^{40}Ar+^{nat}Ag$ system at 27 MeV-A. o , • and □ are for 3 angular experimental measurements[14]. ■ , * , ▲ are the corresponding calculated points.*

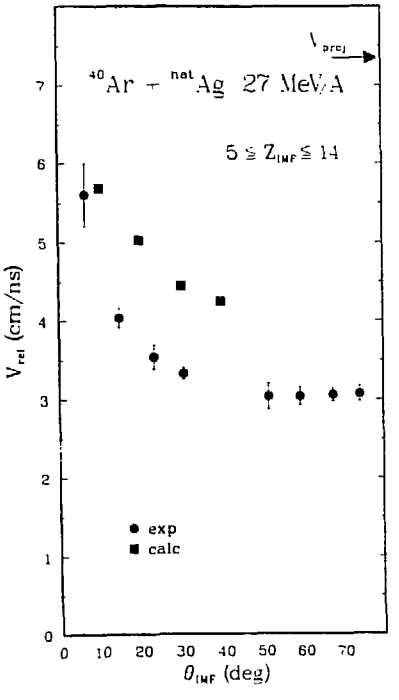

Figure 9

Mean relative velocity of the 2 fragments as a function of the projectile-like detection angle θ_{IMF} in the reaction $^{40}Ar + ^{nat}Ag$ at 27 MeV-A. Full dots • are experimental points[13], full squares ■ are results from simulation.

angular ranges[14]. In the neighbourhood of the grazing angle, the correlation is fairly well reproduced. It must be stressed that, in the model, the positive correlation originates only from the decay of both excited partners, the primary mechanism (transfers) leading to an anti-correlation : the sum of masses remaining constant. For higher angles (figure 8) the tendency towards flattening and inversion of the correlation is reproduced, but the amplitude of the effect is not correct. This discrepancy might be due to an underestimation of the energy dissipation for large angles as already observed at low energies (~ 8 MeV-A). This appears in figure 9, where the relative velocity of the two partners is plotted and compared to the experimental values[13].

The simulation can also compute kinematical correlations. Figure 10 displays the evolution of the target-like recoil angle versus the detected projectile-like mass ($A_P - <\theta_T>$ correlation) and figure 11 shows the same evolution for the recoil velocity $<V_T/c>$. The results of the deep inelastic calculations are plotted with large dots, while the thick line indicates the results

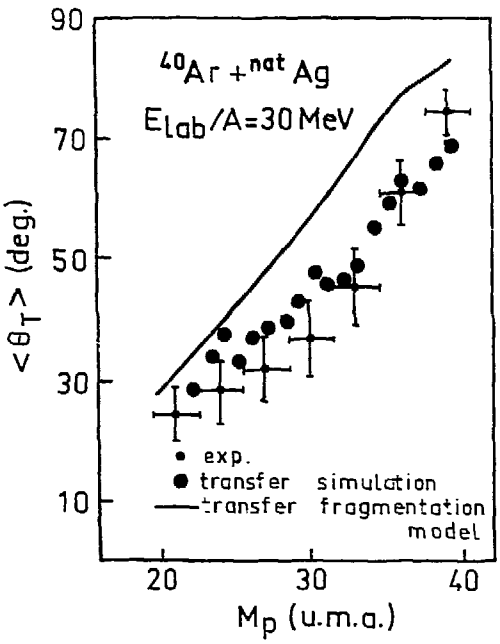

Figure 10

Correlation between projectile-like mass M_P and target-like recoil angle $<\theta_T>$ for the reaction $^{40}Ar+^{nat}Ag$ at 30 MeV-A. Small dots • are experimental points[12], horizontal bars show the selected bins in mass and vertical ones show angle errors. Large dots ● are results from simulation and full line sits for transfer fragmentation model[15].

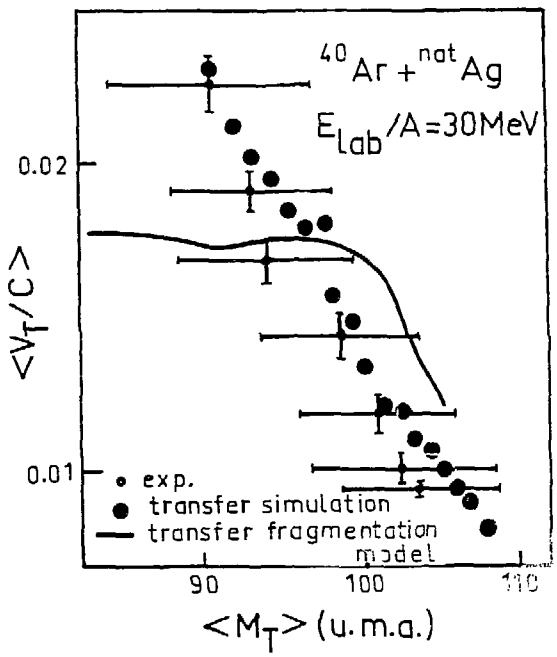

Figure 11

Mean recoil velocity $<v_T/c>$ of target-like fragment as a function of its mean mass $<M_T>$ for the reaction $^{40}Ar + ^{nat}Ag$ at 30 MeV-A. Same symbols as in figure 10, vertical bars are for errors, horizontal bars for standard deviation of mass spectra.

of the dissipative fragmentation model[7,15]. For the two kinematical variables the evolution is well reproduced by the transfer simulation. Higher values of the recoil angle and saturation of the recoil velocity obtained in the dissipative fragmentation framework, seem to reflect a lack of interaction between the two spectators in this model.

3.3. Isotopic distributions

For medium-mass projectiles, like ^{40}Ar, calculations performed in the pure fragmentation framework have proved to be powerful[4] as their predictions are correct for mean values, but also for the tails of isotopic distributions. We have compared the predictions of the simulation for the same informations.

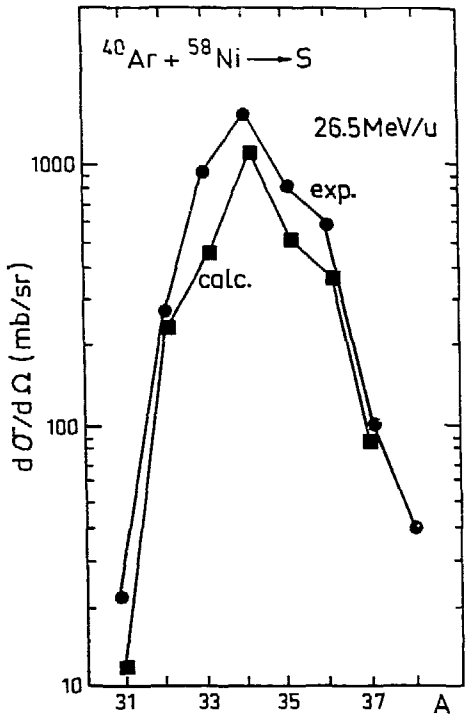

Figure 12

Isotopic distribution for element Z=16 in the reaction $^{40}Ar + ^{58}Ni$ at 26.5 MeV-A. Full dots ● are experimental points[4], full squares ■ are results from simulation without any normalization.

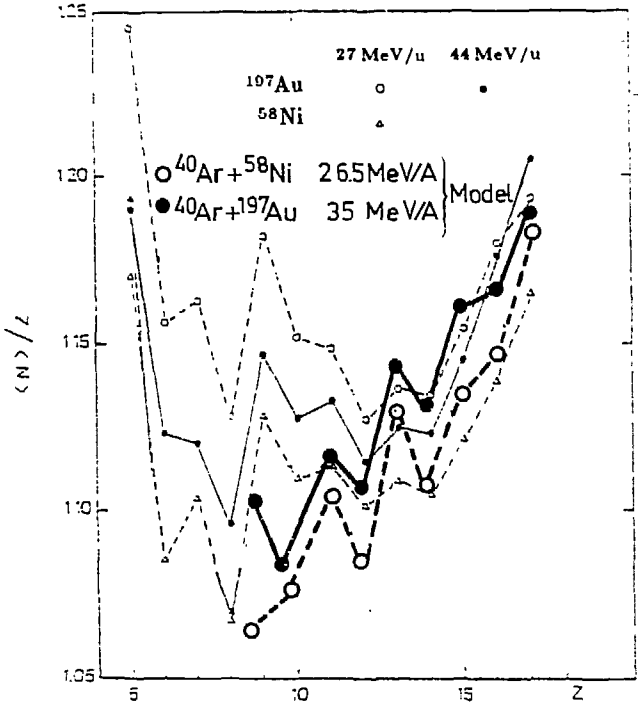

Figure 13

Variation of the N/Z mean value versus Z. Open dots ○ are calculated points for $^{40}Ar + ^{58}Ni$ at 26.5 MeV-A and have to be compared to triangles △ standing for experimental results[4]. Full dots ● are given by the simulation for $^{40}Ar + ^{197}Au$ at 35 MeV-A, they are to be compared to the experimental points : small dots • at 44 MeV-A and small circles ○ at 27 MeV-A.

Figure 12 shows the isotopic distribution of Z=16 for the reaction $^{40}Ar + ^{58}Ni$ at 26.5 MeV-A [4], heavy dots are for experimental points and squares for computed values. In the latter case no normalization factor is introduced. On figure 13 we display the evolution of the $<N>/Z$ ratio for two systems : $^{40}Ar + ^{58}Ni$ at 26.5 MeV-A and $^{40}Ar + ^{197}Au$ at 35 MeV-A. The first one can be directly compared to the data, and the bombarding energy for the latter lies between the experimental ones : 26.5 MeV-A and 44 MeV-A.

The overall decrease of this ratio when the detected fragment departs from the projectile is well reproduced, this reflects the increasing effect of the evaporation striving to pull the residue distribution towards stability. The odd-even oscillation exhibited by the experimental points is also present in the calculations, although the latter amplify the effect. It must be noticed that the occurence of the $<N>/Z$ shift when the ^{58}Ni target is replaced by ^{197}Au is reproduced and

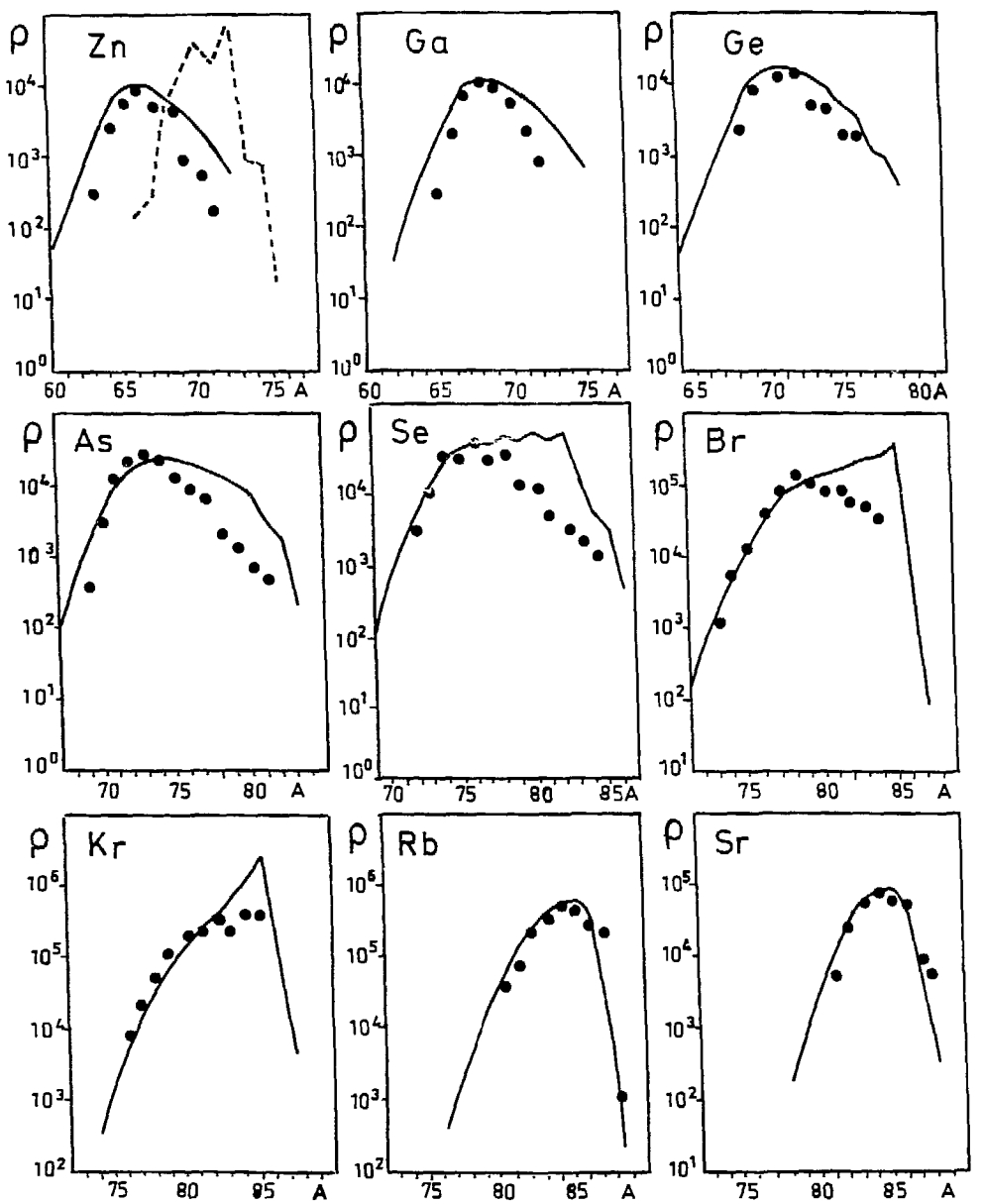

Figure 14

Isotopic distributions at 0° obtained in the reaction $^{86}Kr + ^{27}Al$ at 43 MeV-A. Solid curves show experimental data[6]. Full dots ● are obtained by the simulation after normalization for each Z value. The dashed line represents the result of the fragmentation model for Zn[6].

memory of proton transfers, unlike lighter projectiles.

originates from the enhancement of both neutron transfers towards the projectile and proton transfers into the heavy target.

It was tempting to extend the comparison to isotopic distributions obtained with heavier projectiles, like krypton. The reason for this is that, for such heavy fragments, the sequential decay is dominated by neutron emission. The $<N>/Z$ ratio is then far much sensitive to the excitation energy and the detected Z distribution still contains some characteristics of the primary one.

The experiment has been performed with 43 MeV-A ^{86}Kr ions at GANIL on the LISE line[6], forcing a detection angle close to 0°. For each Z the calculated isotopic distributions were renormalized, then the comparison will not turn on production rates but only on shapes, centroids and widths. On figure 14 are displayed selected isotopic distributions for a ^{27}Al target. Data are indicated by the full line, the transfer simulation by the dots, and the dash line, for the zinc element, shows the results given by the fragmentation model. Clearly the latter fails to reproduce the distribution by all respects. This deviation is due to the strong underestimation of the deposited energy in the fragment, which can show up in isotopic distributions only for such heavy nuclei.

Concerning the transfer simulation, the shapes and centroids are correctly obtained for $Z >$ 36 and $Z < 33$. Nevertheless two deviations are observed : for low Z's the predicted distributions are too narrow : the tails are underestimated. For Z's ranging from 33 to 36 the calculations are unable to reproduce, with the correct yield, the contribution corresponding to the projectile $<N>/Z$ ratio. It is not obvious whether the former effect must be assigned to the treatment of the fragment decay, or to the primary mechanism. The latter deviation clearly shows that the model fails to produce a low excitation energy component. This failure is in agreement with the shift in the energy spectra observed around the grazing angle and already mentioned. The simulation overestimates the energy dissipation around the grazing angle and underestimates it at larger angles.

For the ^{197}Au target the agreement is better since the high $<N>/Z$ contribution is depressed. This may be understood in the following way : for this target the detection angle (0°) if far below the grazing angle ($\approx 4.7°$), in the frame of a deep inelastic collision the system has to rotate and a higher excitation energy is involved.

$$\Delta\delta_1 + \Delta\delta_2 + \Delta E_1^* + \Delta E_2^* + \Delta K + \Delta U = 0 \qquad (1)$$

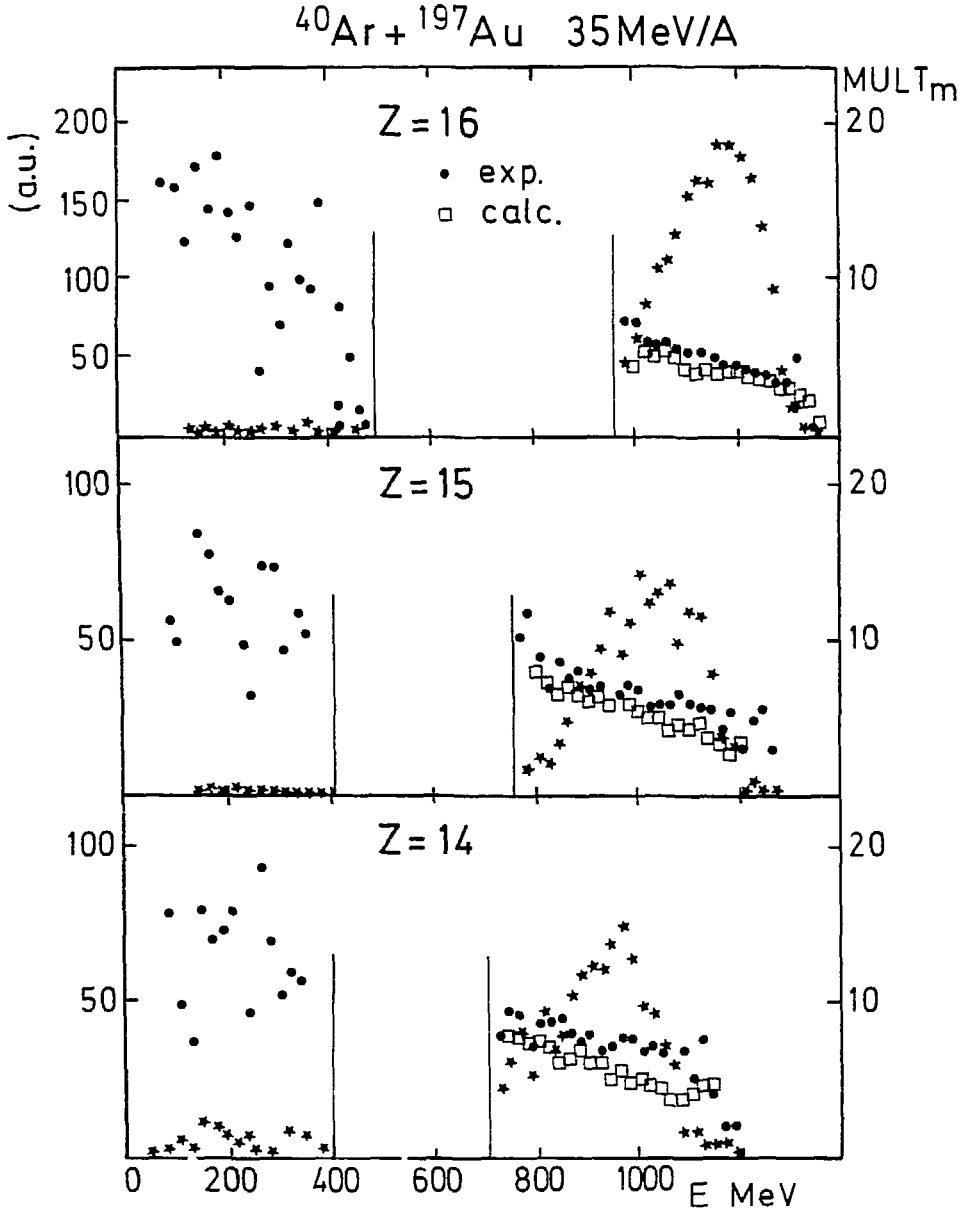

Figure 15

Neutron multiplicity spectra versus kinetic energy of the projectile-like fragment detected in coincidence at 6° for the reaction $^{40}Ar + ^{197}Au$ at 35 MeV-A. For 3 values of projectile-like atomic numbers, stars ★ show their experimental energy spectra, and full dots • the measured multiplicities [17] (right scale). Neutron multiplicities obtained from the simulation are represented by open squares □.

and 2.

3.4. Neutron multiplicities

Morjean et al. have measured neutron multiplicities associated to projectile-like fragments detected around the grazing angle for the $^{40}Ar + ^{197}Au$ system at three bombarding energies : 27, 35 and 44 MeV-A [16]. As the selected target is very heavy and the detector efficiency strongly decreases with the neutron kinetic energy, the measured multiplicities are almost directly related to the excitation energy deposited in the target.

We tried to calculate these multiplicities and compare them to the experimental ones. As the efficiency of the detector strongly depends on the kinetic energy of the neutrons, we chose to correct the calculations for this efficiency. For this purpose the Monte Carlo method allows to follow the decay chain of each partner, then the kinetic energy and angle of each emitted neutron has been computed and a detection probability has been evaluated from the efficiency curve. For this energy dependent efficiency, the neutron source was assumed isotropic [16]. This procedure allows direct comparison to measured multiplicities.

Figure 15 shows, for three elements, the dependence of the multiplicity on the kinetic energy of the fragment detected at 6°. In this case, the bombarding energy is 35 MeV-A [17]. The general behaviour is fairly well reproduced, in particular the steep rise in the high part of the energy spectrum and the smooth slope for larger dissipations. The absolute values are also correct, although a slight trend to underestimate the multiplicity seems to show up for Z's far from the projectile.

Data for all masses may be gathered by averaging the multiplicity over the whole energy spectrum. We then obtain a dependence of the multiplicity on the projectile-like mass. The comparison is reported on figure 16, where results of the transfer-fragmentation model are also presented [15]. Data and calculations are now related to the 27 MeV-A incident energy. The slight underestimation for low masses ($\approx 15\%$) is confirmed. In spite of this deviation, the comparison is satisfactory : the shape of the curve is well reproduced, particularly for the low mass region where the flattening of the mean multiplicity is obtained. Furthermore experimental results have shown to be independent on the projectile energy [16] between 27 MeV-A and 44 MeV-A, when the projectile-like product is detected close to the grazing angle. This independence is also a main feature of the deep inelastic simulation which, for the correlation displayed on figure 16, leads to identical results at 27 MeV-A and 35 MeV-A. In the framework of the model, this behaviour may be understood as follows : the transfer flux, for the high velocities here involved, is almost sym-

ϵ_2, m_1, m_2, and then from equations (2)-(4) all the variations of angular momentum and energies.

metrical, then the excitation energy is equally shared. This introduces a strong correlation between the number of neutrons emitted from the target and the total mass evaporated by the projectile-like fragment. This latter quantity may be approximately related to the difference between projectile and detected mass, since the primary mass distribution is narrow.

It must be noticed that for masses higher than 22 the prediction of the transfer-fragmentation model also follows the experimental values. But the reason for this is completely different : in this framework, the heating of the two partners is also achieved through transfers. Then half of this energy is deposited in the fire ball, the remaining part being distributed among the spectators according to their masses. This energy sharing leads to target-like excitation energies comparable to those given by the pure transfer calculation which roughly complies with an equipartition law. On the other hand, excitation energies stored in the light projectile-like fragment are found completely different in the two models.

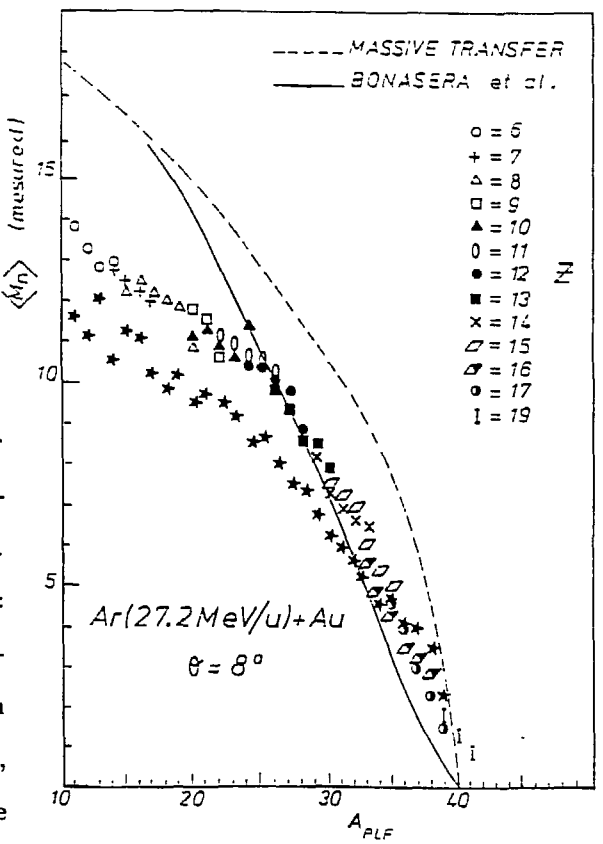

Figure 16

Mean neutron multiplicity versus projectile-like mass. Measurements are performed at 8° for the reaction $^{40}Ar + ^{197}Au$ at 27 MeV-A [5]. Stars ⋆ represent the result of our simulation, other symbols are for the different detected isotopes. The solid line shows the result of the transfer fragmentation model [16]. The simulation gives identical results for 27 MeV-A and 35 MeV-A reactions.

4. Discussion and conclusions

In order to appreciate the importance of transfers for reactions around the Fermi energy, we tried to re-analyze a set of experimental data generally interpreted, up to now, in a fragmentation framework. For this purpose we used a model based on the main assumption that transfers are the dominant process for energy and angular momentum dissipation.

We applied an evaporation code taking only account of neutron, proton and alpha emission. At

The salient point of the comparison is that the simulation is able to reconcile some experimental findings often assigned to a fragmentation mechanism (high velocities for the projectile-like fragment, positive mass-mass correlation) and others supposed to originate from more central collisions (high neutron multiplicities). Furthermore, in this context, some unsolved aspects receive a natural explanation : asymmetric shape of the energy spectra with a tail towards low energies, ratio of perpendicular to parallel momentum widths, target effect on isotopic distributions and dependence of their mean value on the considered element, flattening of the neutron multiplicity curve for low kinetic energies or low masses of the projectile-like product. A satisfactory agreement is also obtained for correlated quantities measured in coincidence experiments.

Nevertheless, this model clearly shows up systematic deviations from experimental data. The first one deals with the angular dependence of the dissipation. We have already mentioned that the dissipated energy is underestimated beyond the grazing angle. This is not a specific problem of this energy range as it is also present at low bombarding energy where the deep inelastic process dominates. Rather it reveals a weakness of the model, which can be clearly pointed as a lack of radial friction in the separation stage of the two partners. As *only* nucleons which are *directed* towards the window can be transferred, dissipation is strongly suppressed in this stage as it is supported by energy considerations. Therefore the system hardly sticks together while it rotates. This is probably an indication that the neglect of other ways for dissipation, like mutual excitation, is not justified.

The other main disagreement can be expressed as the reluctance put up by the calculation to produce low excited nuclei around the grazing angle. This has been illustrated by the shift in the energy spectra, the momentum widths and isotopic distributions for ^{86}Kr projectiles. This feature requires a modification of the involved mechanism. Is it necessary to call on fragmentation ? Before concluding on this point we must have in mind, as mentioned in Section 2, that transfers do not necessarily act in the same way around 30 MeV-A and above as they do at lower energies. It is likely that in the Fermi energy range, due to the high velocity mismatch, many transferred nucleons may escape from the acceptor nucleus giving rise to a preequilibrium emission, so that only a part of the carried momentum and energy is deposited in the nucleus.

Included, in the model, the treatment of this phenomenon would certainly improve the comparison with the data for energy spectra and isotopic distributions. The question is now : how would results be changed concerning other quantities as projectile-like target-like correlations or

t e istogram . t mus e no ice a *no norma isa ion ac or* is use , e i eren ia cross section is given by the simulation.

neutron multiplicities ? The answer is not obvious as it appears from the following considerations. For a given detected mass, the primary excitation energy would be lower, but the number of transferred nucleons required to reach it would be larger, at least for fragment masses far away from the projectile mass. This results from the fact that, due to sequential decay, full absorption of the transferred nucleon is more efficient to lowering the mass than escaping transfer. The kinematical implications of this effect are not easily predictable. Now one may think that preequilibrium emission would decrease the neutron multiplicities, emphasizing the slight underestimation we observed. This is not necessarily the case for two reasons. Firstly because preequilibrium neutrons may contribute significantly to the multiplicity, as part of them travel with low velocities in the laboratory system. Moreover, for a given detected mass, we already noticed that the number of exchanged nucleons might be increased when they have the possibility to escape. Now for very asymmetric systems, the transparency of the heavy target could be lower than that of the light projectile, leading to approximately the same excitation energy.

This means that a true simulation with realistic parameters is needed and must be compared to a large set of data including results from experiments in which particles are detected in coincidence with massive fragments.

The comparison we have reported supports the idea that transfers still play a dominant role in the energy range here considered. This means that the usual picture of two slightly excited spectators associated to a fireball is unlikely to occur, because the conditions for such a mechanism are conflicting with those for transfers. However the presence of a more general fragmentation process is neither asserted nor invalidated. As possible means to bring an answer to this problem, we suggest an improvement of the model, taking account of the specific behaviour of transfers at high relative velocity : preequilibrium emission after transfer. A new confrontation to the data would eventually reveal the necessity to call on other mechanisms.

of the energy spectra for the $^{40}Ar + ^{27}Al$ system at 44 MeV-A [2]. In this latter case, the agreement is better if one notes that the energy scale is expanded. However the same general behaviour

REFERENCES

1) *D. Guerreau*, Nucl. Phys. **A447** (1985) 37c

2) *R. Dayras et al.*, Nucl. Phys. **A460** (1986) 299

3) *F. Rami, J.P. Coffin, G. Guillaume, B. Heusch, P. Wagner, A. Fahli, P. Fintz*, Z. Phys. **A318** (1984) 239

4) *V. Borrel, B.Gatty, D. Guerreau, J. Galin and D. Jacquet*, Z. Phys. **A324** (1986) 205

5) *M. Morjean et al.*, Phys. Lett. **203B** (1988) 215

6) *D. Bazin*, Thesis Université de Caen, July 1, 1989, *unpublished*

7) *A. Bonasera, M. Di Toro, C. Grégoire*, Nucl. Phys. **A463** (1987) 653

8) *S. K. Samaddar, J. N. De and K. Krishan*, Phvs. Rev. **C31** (1985) 1053

9) *L. Tassan-Got*, Thesis Université Paris Sud, June 27, 1988, *unpublished*

10) *J. Randrup*, Nucl. Phys. **A307** (1978) 319
J. Randrup, Nucl. Phys. **A327** (1979) 490

11) *A. S. Goldhaber*, Phys. Lett. **53B** (1974) 306

12) *F. Gadi Dayras*, thesis Université Paris Sud, June 23, 1988, *unpublished*

13) *B. Borderie, M. Montoya, M. F. Rivet, D. Jouan, C. Cabot, H. Fuchs, D. Gardès, H. Gauvin, D. Jacquet, F. Monnet, F. Hanappe*, Phys. Lett. **205B** (1988) 26

14) *B. Borderie, M. Montoya, M. F. Rivet, D. Jouan, C. Cabot, H. Fuchs, D. Gardès, H. Gauvin, D. Jacquet, F. Monnet, F. Hanappe*, Nouvelles du Ganil **22** (1987) 13

15) *A. Adorno, F. Gulminelli, A. Bonasera, M. Di Toro, C. Grégoire*, XXVI International Winter Meeting on Nuclear Physics, Bormio, January 25-30, 1988

16) *J. Galin et al.*, XXVI International Winter Meeting on Nuclear Physics, Bormio, January 25-30, 1988

17) *M. Morjean and D. Jacquet*, private communication